

Supporting Information for "Fast local warming of sea-surface is the main factor of recent deoxygenation in the Arabian Sea"

Zouhair Lachkar¹, Michael Mehari¹, Muchamad Al Azhar^{1,4}, Marina Lévy², and Shafer Smith^{1,3}

¹Center for Prototype Climate Modeling, New York University Abu Dhabi, Abu Dhabi, UAE

²Sorbonne Université (CNRS/IRD/MNHN), LOCEAN-IPSL, Paris, France

³Courant Institute of Mathematical Sciences, New York University, New York, USA

⁴Plymouth Marine Laboratory, Plymouth, UK

Correspondence: Zouhair Lachkar (zouhair.lachkar@nyu.edu)

Analysis of model drift

In order to analyze the model drift, we show the AS domain-averaged salinity and O₂ in the top 200 m and between 200 and 1000 m in the climatological simulation and over the 4 cycles of interannual forcings (Fig S2 and Fig S3). In the top 200 m, the drift in salinity becomes very small already by the end of the climatological integration. During the interannual forcing integration, the average salinity over the 29 year period remains stable across the different integration cycles (Fig S2). Below 200m, the salinity drift decreases over time and becomes very limited by the end of the internannual forcing integration, with an average salinity drop between the 3rd and the 4th cycle of less than 0.001 psu (Fig S2). In the top 200 m, the AS domain-averaged O₂ initially drops rapidly but then slowly increases after the first 30 years of the climatological forcing integration. During the interannual forcing integration period, the oxygenation trend continues although at a weaker rate, with O₂ increasing by 1.2 mmol m⁻³ between the 1st and the 4th cycle (Fig S3). Below 200 m, O₂ increases initially at a relatively fast rate (15 mmol m⁻³ decade⁻¹), but this rate slows down by the end of the climatological forcing period to (0.6 mmol m⁻³ decade⁻¹) and a quasi-stabilization by the end of the interannual forcing integration (Fig S3). As a result of the model drift during the climatological integration, the OMZ volume initially expands over the first 30 years of integration but slowly and continually shrinks afterwards (Fig S4). During the interannual forcing period, the volume of the OMZ displays larger interannual variations but is relatively stable between the different integration cycles (Fig S4). Contrasting the local trends in both the top 200 m and between 200 m and 1000 m in the last 29 years of the climatological integration to those from the last interannual cycle (control hindcast run) reveals that the O₂ trends purely driven by model drift in the climatological run are positive in most regions, contrasting with the negative trends obtained in the interannual control simulation (Fig S5). This indicates that our deoxygenation rate estimates are rather conservative and can be larger when correcting with the potential model drift.

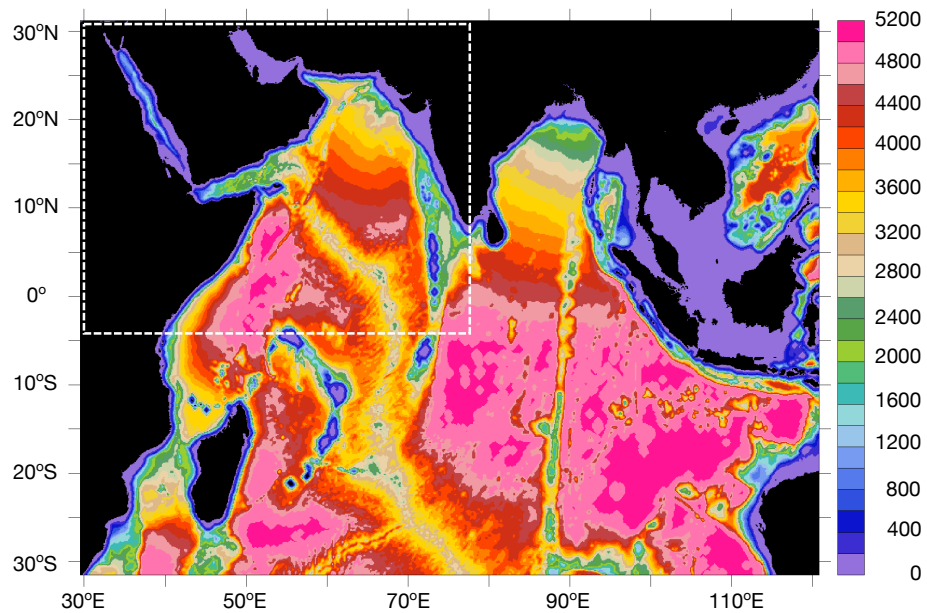


Figure S1. Model domain and seafloor bathymetry. The model domain covers the full Indian Ocean from 31°S to 31°N and 30°E to 120°E. The color shading shows the sea floor bathymetry (in m). The white dashed square highlights the region of interest used for the analysis and plots throughout the whole paper (5°S to 30°N and 32°E to 78°W).

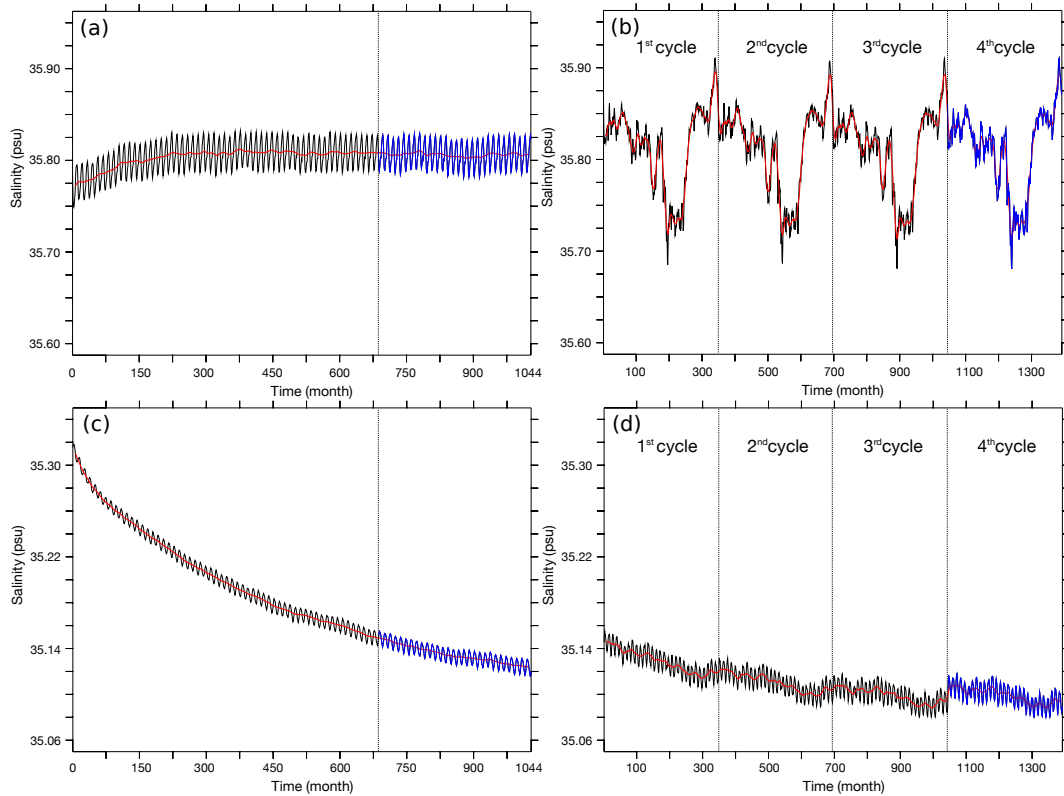


Figure S2. Model salinity drift. Arabian Sea averaged salinity in the top 200 m (a-b) and between 200m and 1000m (c-d) as simulated by the model as a function of time (black curve). The low-pass filtered data are shown in red. Left panels (a-c) show salinity as simulated under climatological forcing (climatological run) and right panels (b-d) indicate the evolution of salinity under repeated four cycles of ERA forcing. The last 29 years of the climatological run as well as the (29 year long) last cycle of the hindcast run are highlighted in blue.

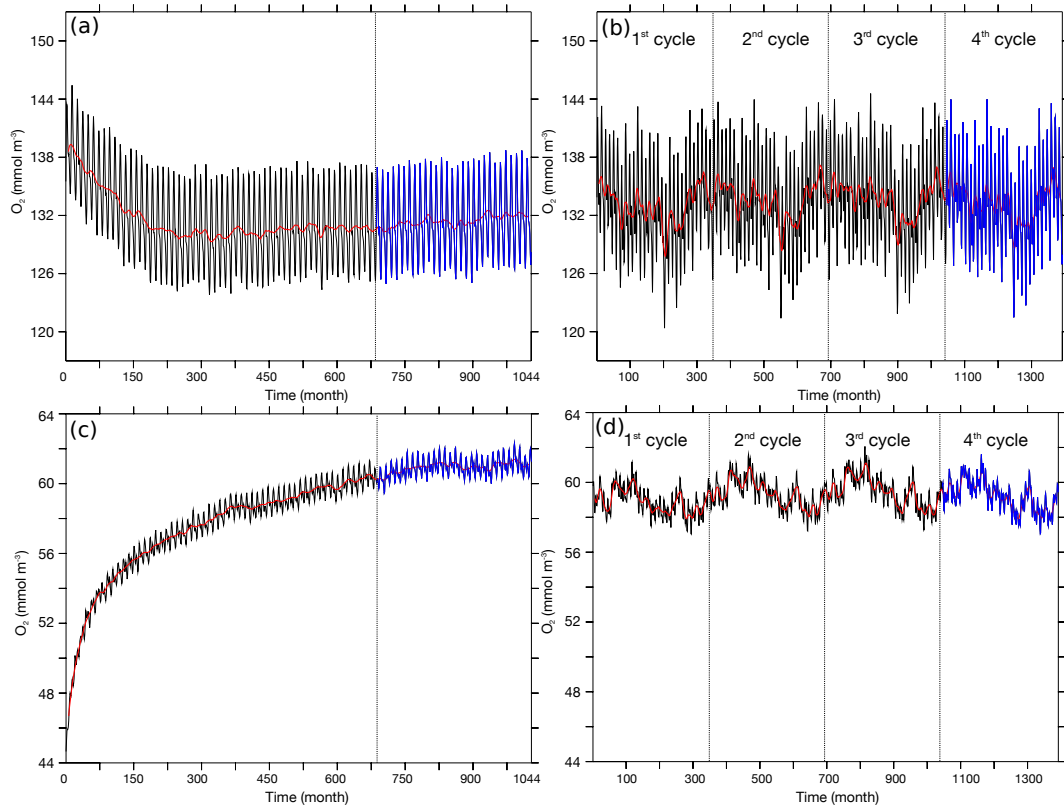


Figure S3. Model oxygen drift. Arabian Sea averaged oxygen in the top 200 m (a-b) and between 200m and 1000m (c-d) as simulated by the model as a function of time (black curve). The low-pass filtered data are shown in red. Left panels (a-c) show O_2 as simulated under climatological forcing (climatological run) and right panels (b-d) indicate the evolution of O_2 under repeated four cycles of ERA forcing. The last 29 years of the climatological run as well as the (29 year long) last cycle of the hindcast run are highlighted in blue.

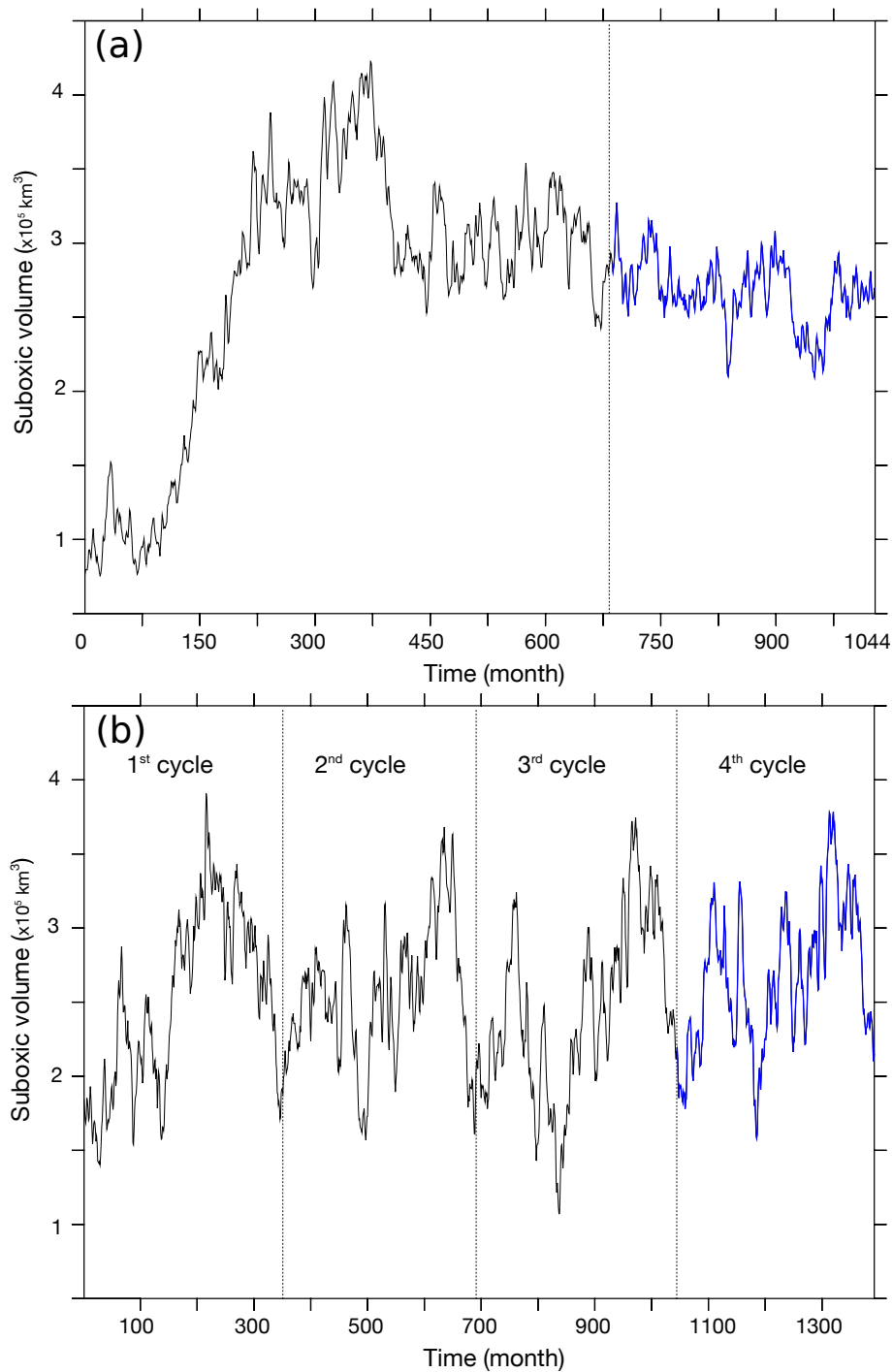


Figure S4. Model suboxic volume drift. Arabian Sea total suboxic volume as a function of time (black curve) as simulated by the model under (a) climatological forcing and (b) under repeated four cycles of interannual ERA forcing. The last 29 years of the climatological run as well as the (29 year long) last cycle of the hindcast run are highlighted in blue.

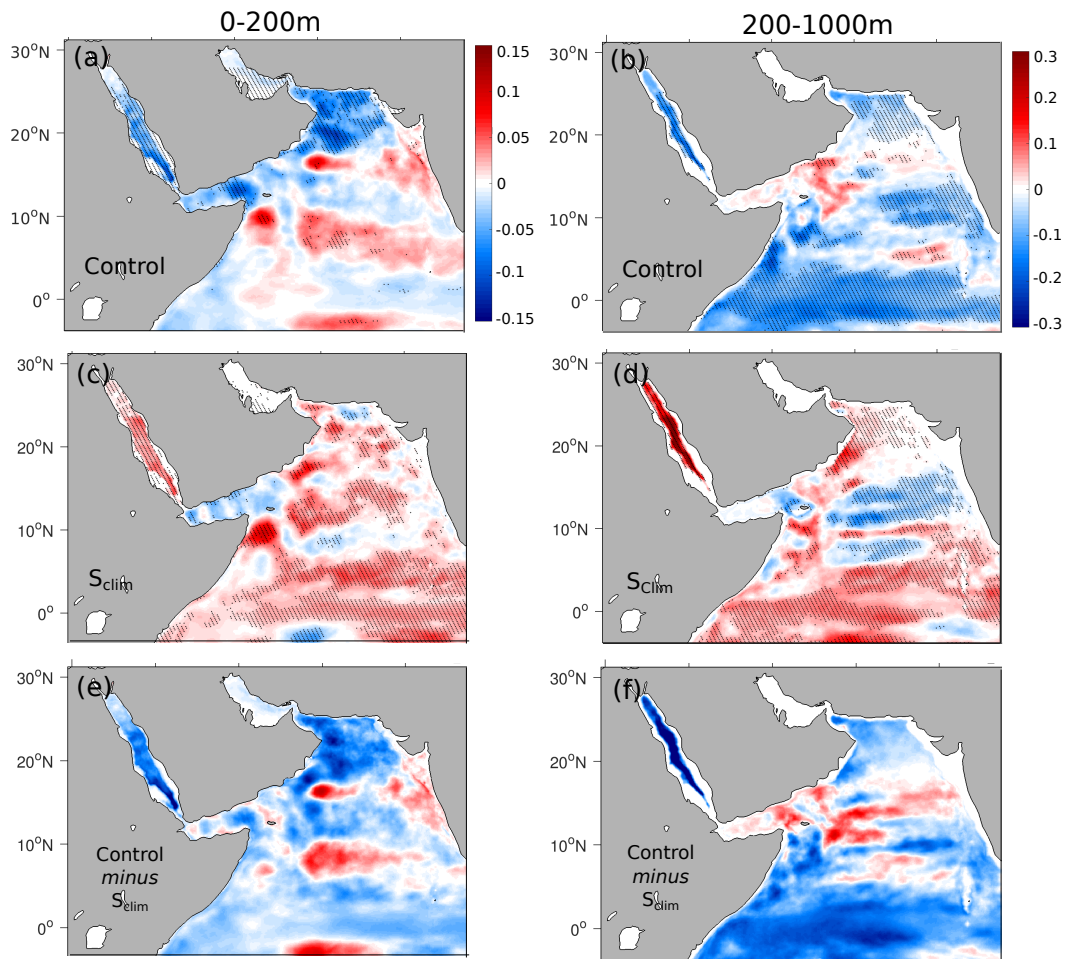


Figure S5. Deoxygenation rates in the hindcast simulation relative to the climatological run. Trends in O₂ inventories (in Gmol decade⁻¹) in (left) the top 200 m and (right) the 200-1000 m layer in the control hindcast simulation (top), the last 29 years of the climatological simulation (middle) and the difference between these trends (bottom). Statistically significant trends at 95% confidence interval following a Mann-Kendall (MK) test are represented by hatching.

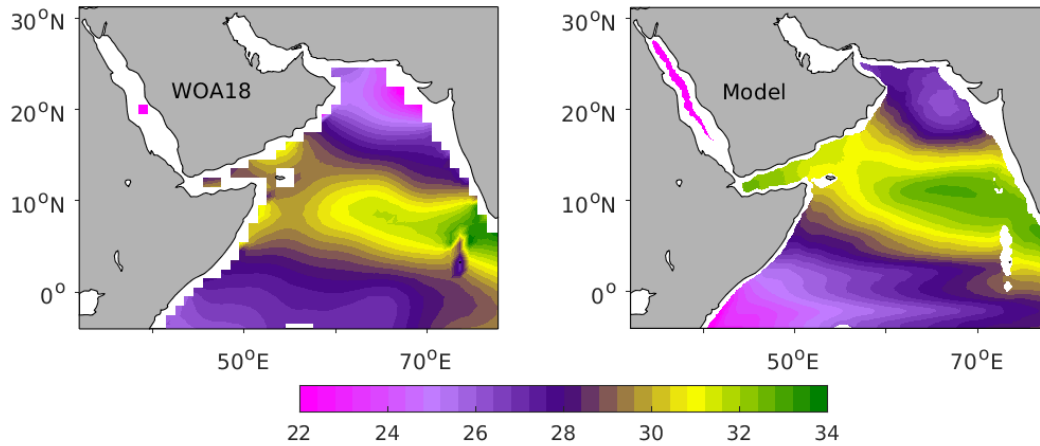


Figure S6. Evaluation of model simulated subsurface nitrate Annual mean NO_3^- averaged between 250 m and 700 m (in mmol m^{-3}) as simulated in the model (right) and from the WOA-2018 dataset (left).

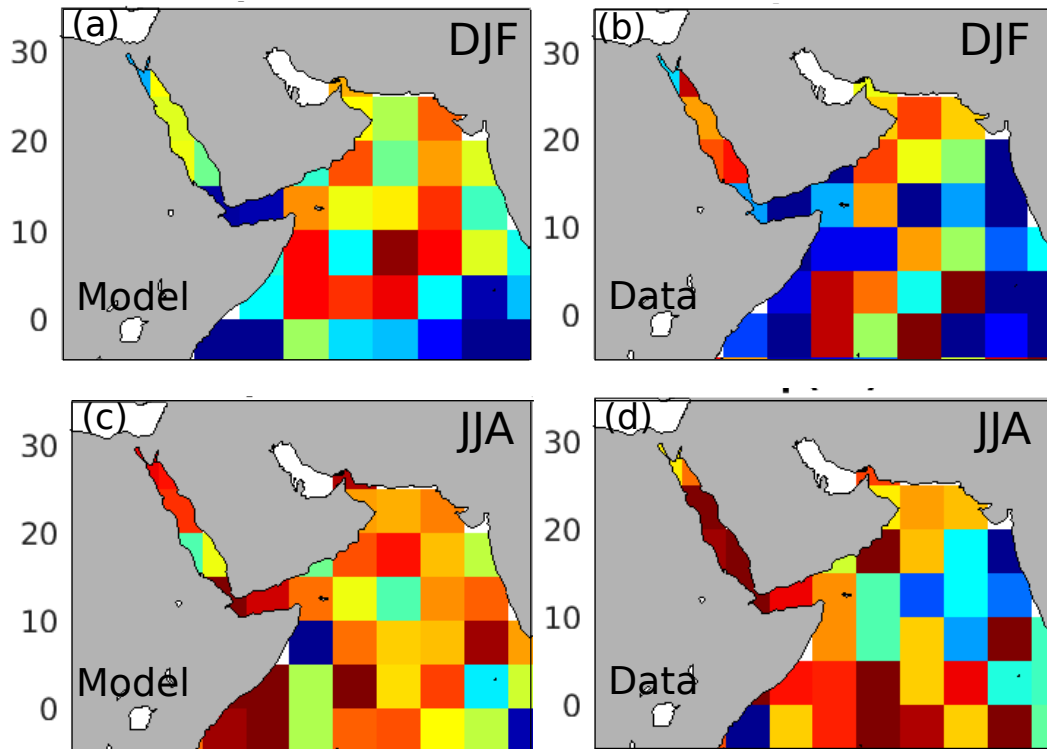


Figure S7. Long-term changes in temperature at 100 m. change in winter (top) and summer (bottom) temperature at 100 m depth between the first five years (1982-1986) and the last five years (2006-2010) of the study period. In-situ observations from the World Ocean Database (2018) were binned seasonally on a 5x5 horizontal grid at each standard depth. The changes are derived from seasonal climatologies computed for the (1982-1986) and (2006-2010) periods.

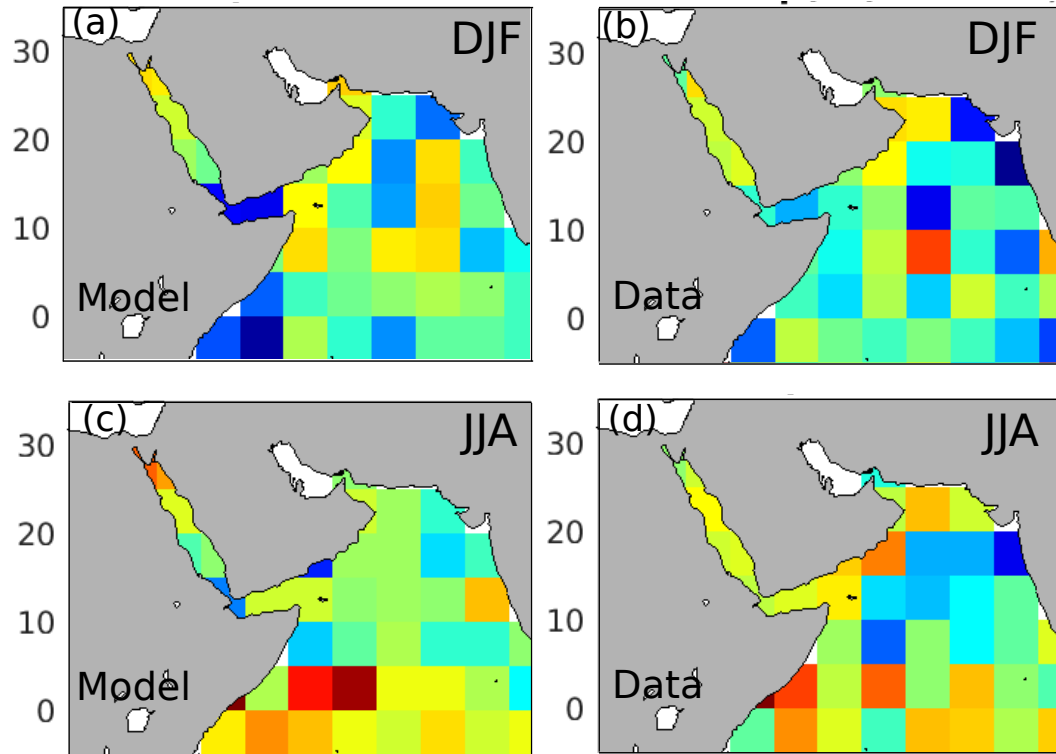


Figure S8. Long-term changes in temperature at 200 m. change in winter (top) and summer (bottom) temperature at 100 m depth between the first five years (1982-1986) and the last five years (2006-2010) of the study period. In-situ observations from the World Ocean Database (2018) were binned seasonally on a 5x5 horizontal grid at each standard depth. The changes are derived from seasonal climatologies computed for the (1982-1986) and (2006-2010) periods.

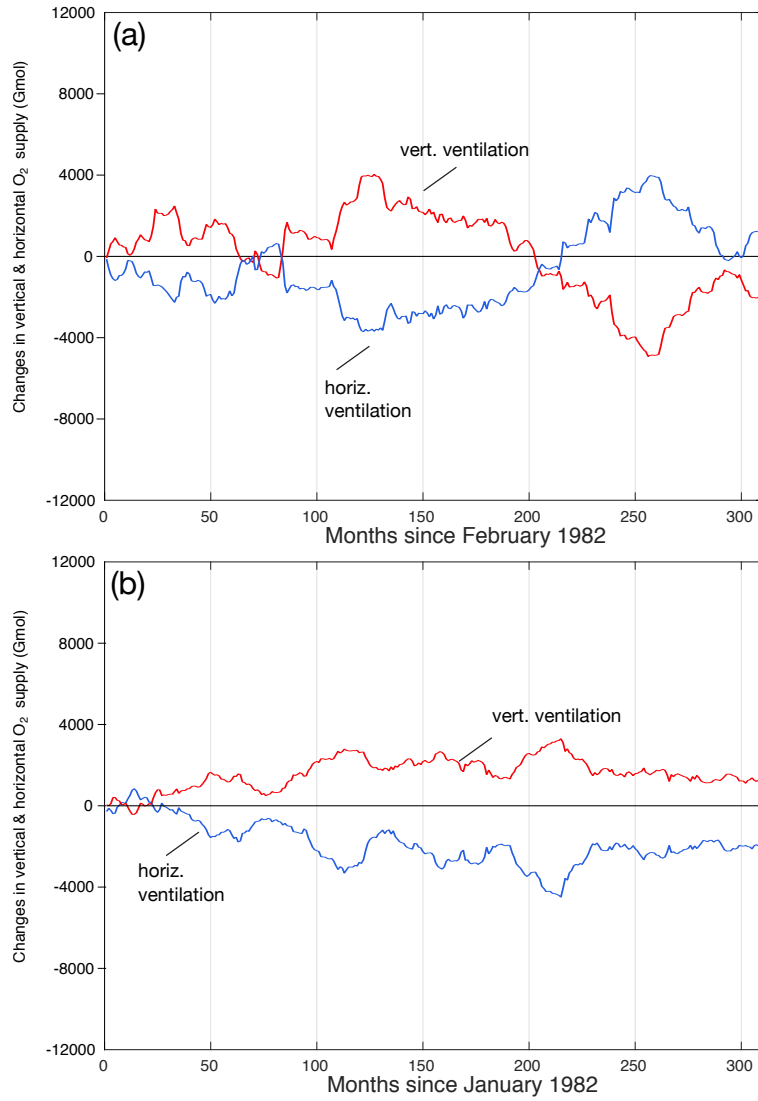


Figure S9. Role of vertical and lateral ventilation changes in Arabian Sea deoxygenation. Cumulative contributions of vertical (red) and horizontal (blue) ventilation changes to O_2 anomalies in (a) the (100-200 m) subsurface and (b) the intermediate (200-1000 m) ocean.

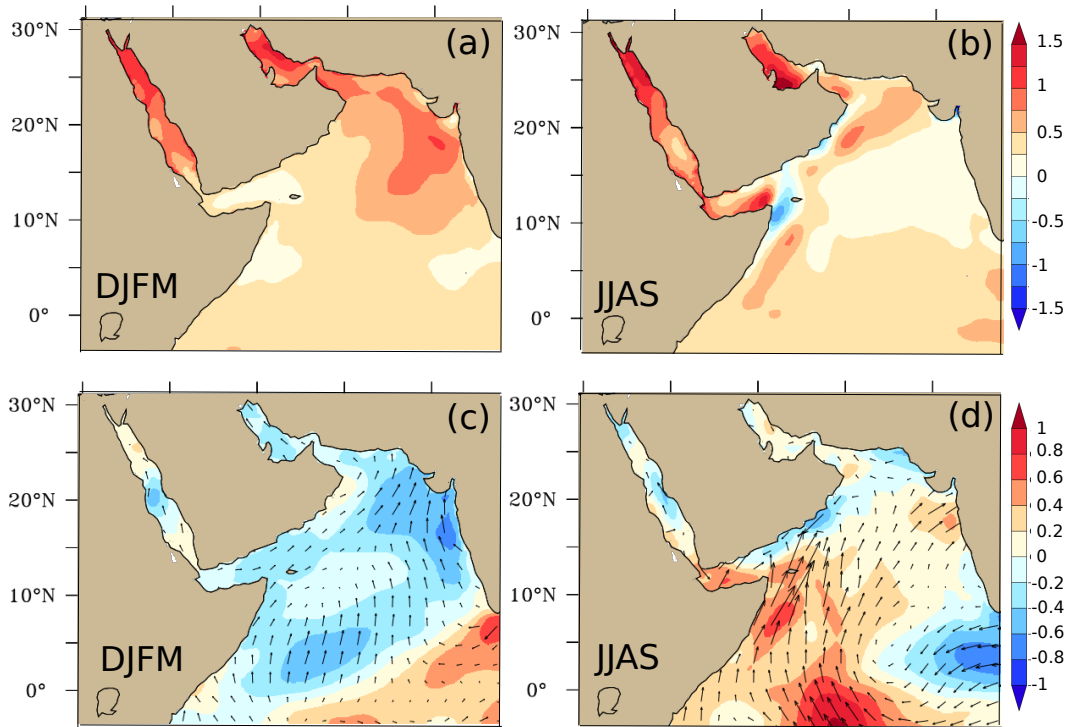


Figure S10. Long-term changes in atmospheric forcing. change in (left) winter and (right) summer (top) sea surface temperature (in °C) and (bottom) surface winds (color shading indicates changes in wind speed in m s^{-1} whereas arrows show changes in wind stress vector) between the first five years (1982-1986) and the last five years (2006-2010) of the study period.

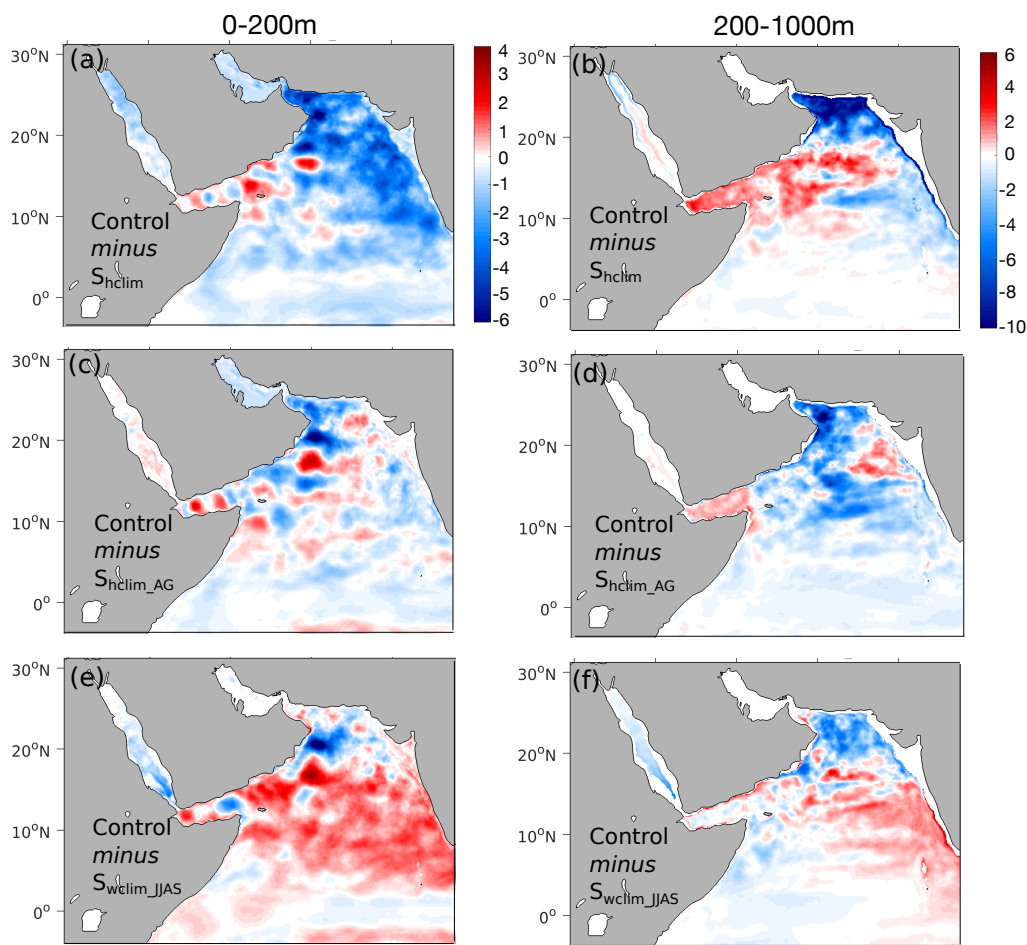


Figure S11. Effects of different atmospheric forcing perturbations on deoxygenation rates. Difference in O_2 inventory trends between the control run and the S_{hclim} , S_{hclim_AG} and S_{wclim_JJAS} sensitivity simulations in (left) the top 200 m and (right) the 200-1000 m layer (in % decade⁻¹). Statistically significant trends at 95% confidence interval following a Mann-Kendall (MK) test are represented by hatching.

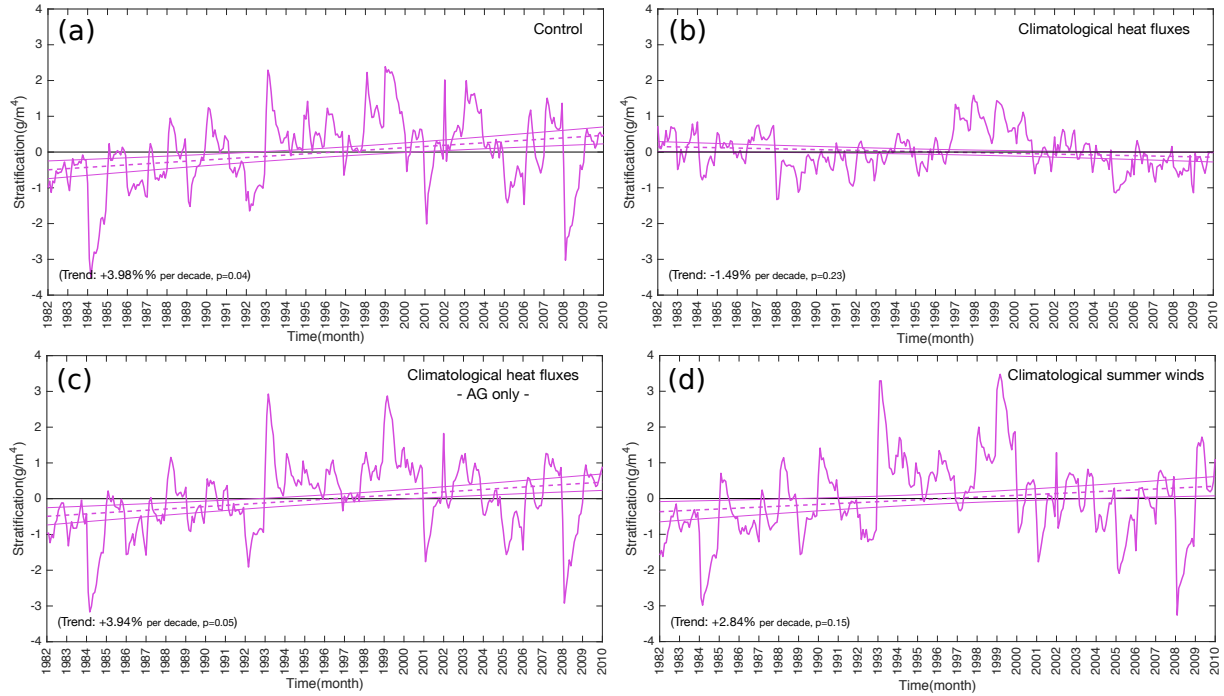


Figure S12. Vertical stratification under different atmospheric forcing scenarios. Vertical stratification at 200 m (in g m^{-4}) averaged across the Arabian Sea as a function of time in the control (a) and (b-d) the S_{hclim} , $S_{\text{hclim_AG}}$ and $S_{\text{wclim_JJAS}}$ sensitivity simulations. The dashed lines indicate the corresponding trend lines.

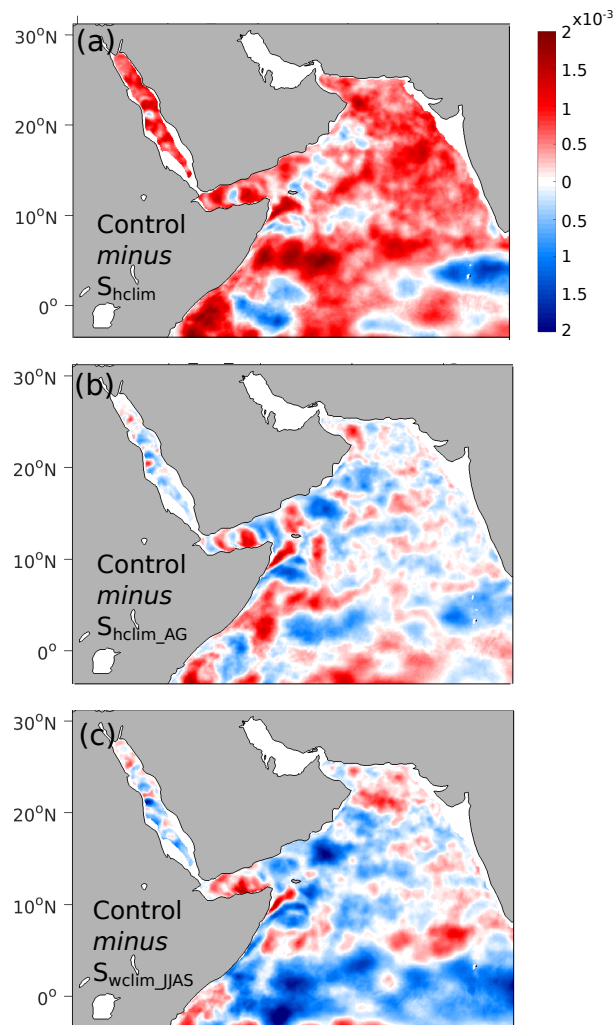


Figure S13. Effects of different atmospheric forcing perturbations on vertical stratification. Difference in vertical stratification trends at 200 m (in $\text{g m}^{-4} \text{decade}^{-1}$) between the control run and the S_{hclim} , S_{hclim_AG} and S_{wclim_JJAS} sensitivity simulations. Statistically significant trends at 95% confidence interval following a Mann-Kendall (MK) test are represented by hatching.

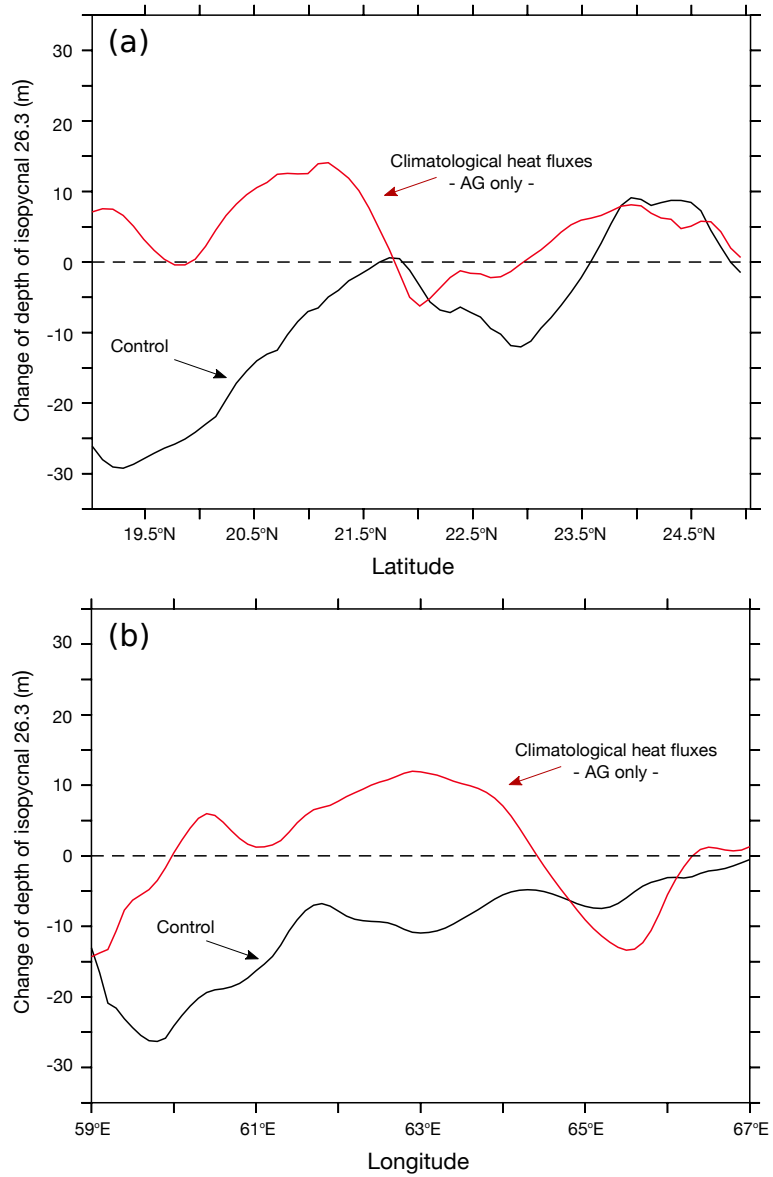


Figure S14. Depth of spreading of the Gulf waters. Change in the depth of isopycnal 26.3, corresponding to the Gulf water potential density, (in m) between the first five years (1982-1986) and the last five years (2006-2010) of the study period in the control (black) and in the S_{helim_AG} (red) runs along (top) 60°E and (bottom) 20°N in the northern Arabian Sea.

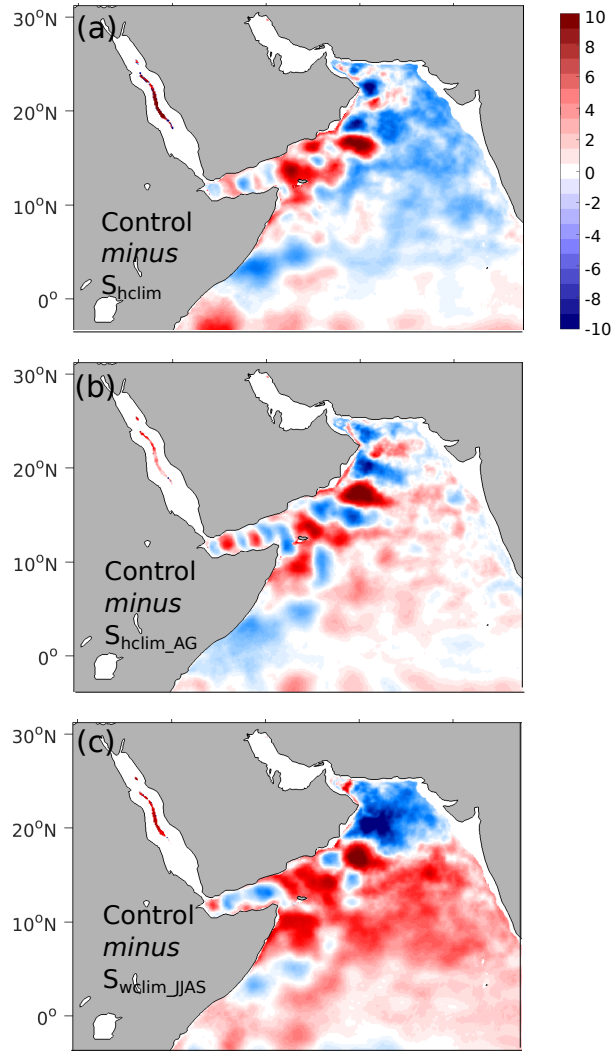


Figure S15. Effects of different atmospheric forcing perturbations on thermocline depth. Difference in depth of isotherm 20°C trends (in m decade⁻¹) between the control run and the S_{hclim}, S_{hclim_AG} and S_{wclim_JJAS} sensitivity simulations. Statistically significant trends at 95% confidence interval following a Mann-Kendall (MK) test are represented by hatching.

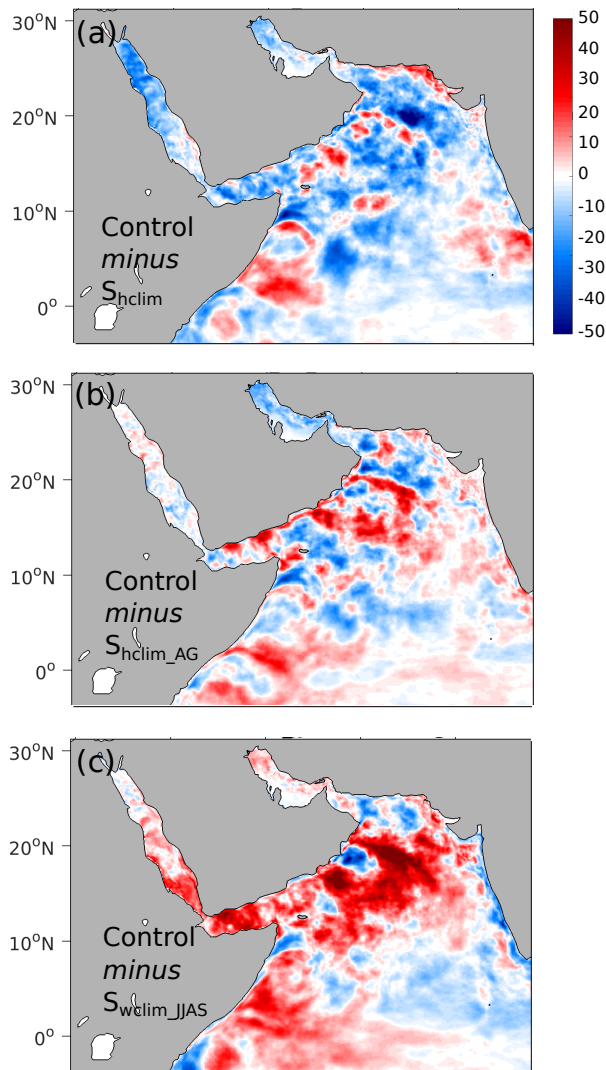


Figure S16. Effects of different atmospheric forcing perturbations on net primary production. Difference in net primary production trends (in $\text{mol m}^{-2} \text{ yr}^{-1} \text{ decade}^{-1}$) between the control run and the S_{hclim} , S_{hclim_AG} and S_{wclim_JJAS} sensitivity simulations. Statistically significant trends at 95% confidence interval following a Mann-Kendall (MK) test are represented by hatching.

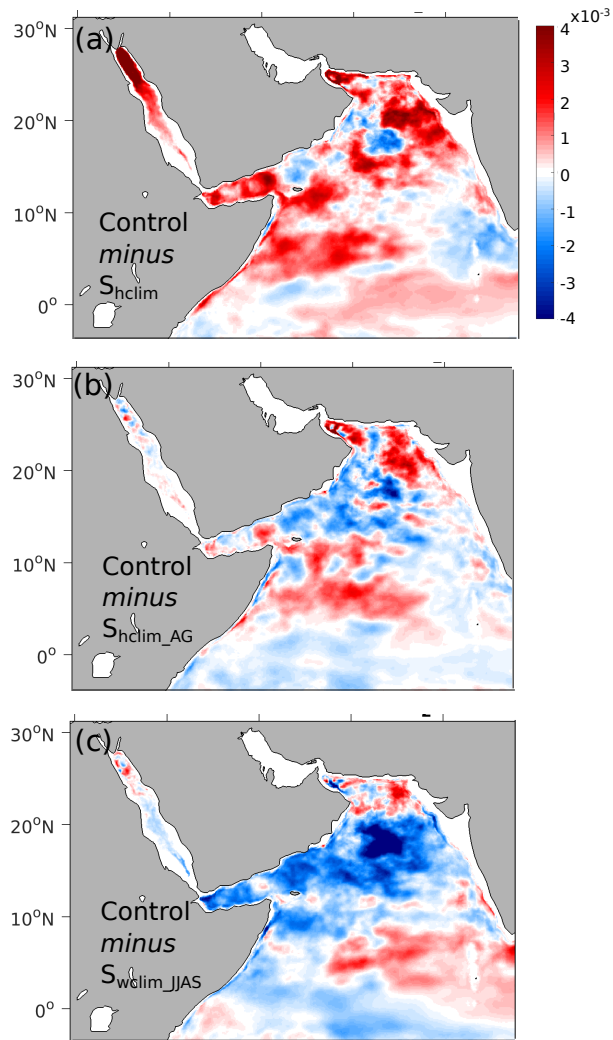


Figure S17. Effects of different atmospheric forcing perturbations on O_2 biological consumption. Difference in trends in O_2 consumption due to remineralization (in $\text{mmol m}^{-2} \text{s}^{-1} \text{decade}^{-1}$) in the 200-1000 m layer between the control run and the S_{hclim} , S_{hclim_AG} and S_{wclim_JJAS} sensitivity simulations. Statistically significant trends at 95% confidence interval following a Mann-Kendall (MK) test are represented by hatching.

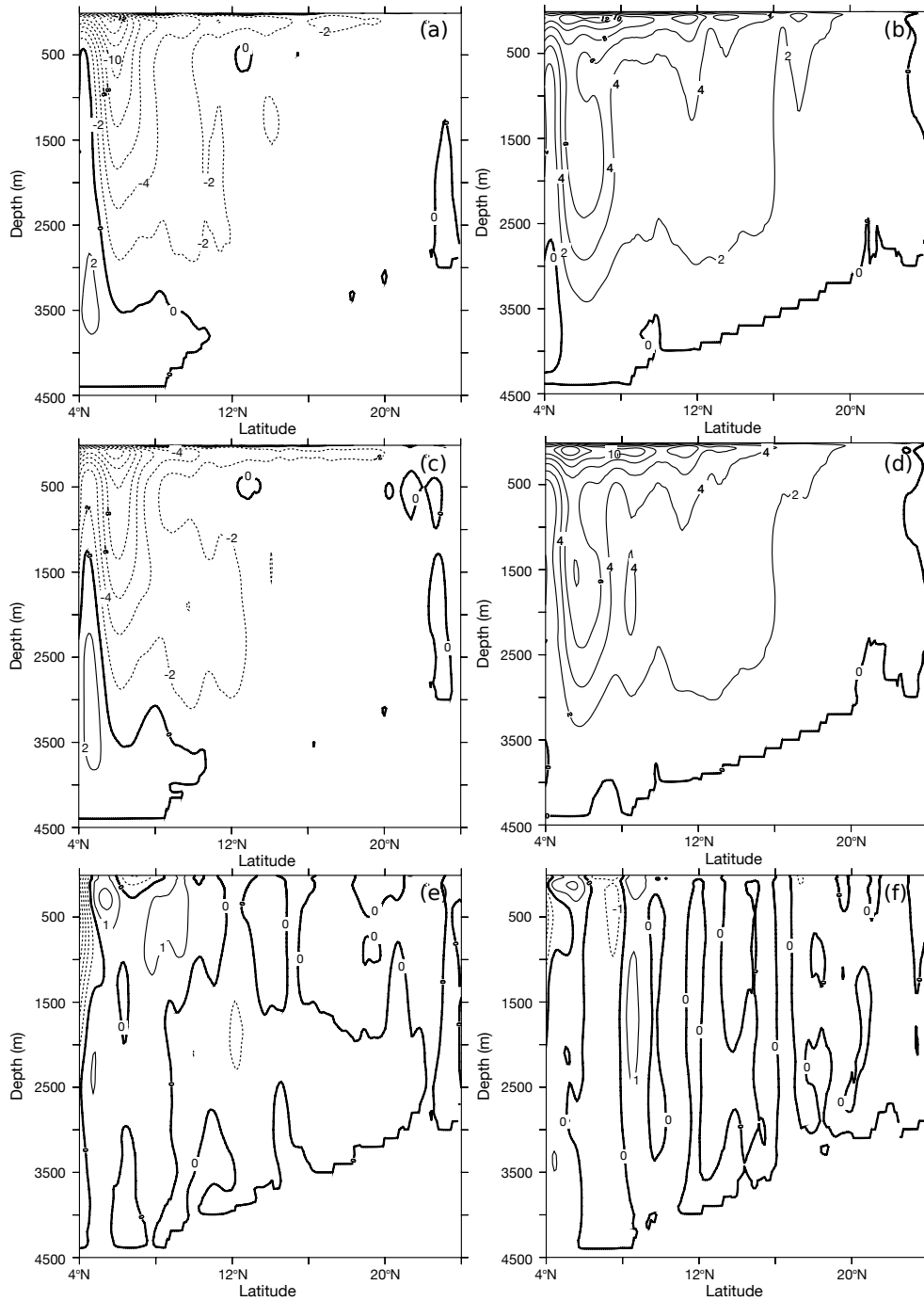


Figure S18. Meridional stream function in the Arabian Sea. Meridional stream function (in Sv) in the Arabian Sea in winter (left) and summer (right) monsoon seasons in (top) the first five years (1982-1986), (middle) the last five years (2006-2010) and (bottom) the change between the two periods (positive indicates clockwise circulation).

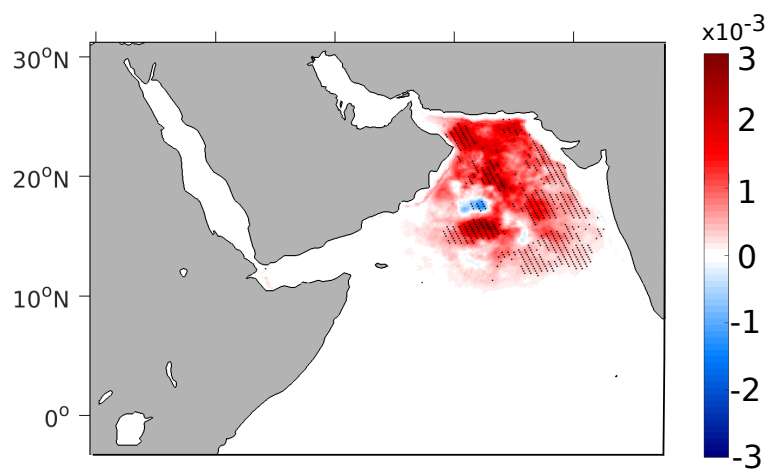


Figure S19. O₂ changes driven by denitrification Trends in O₂ between 200 and 1000 m (in $\text{mmol m}^{-2} \text{s}^{-1} \text{decade}^{-1}$) driven by change in denitrification. Statistically significant trends at 95% confidence interval following a Mann-Kendall (MK) test are represented by hatching.